Estimating the effective elastic thickness of the lithosphere of the Iberian peninsula based on multitaper spectral analysis

D. Gómez-Ortiz,[1,2] R. Tejero,[2] J. Ruiz,[2] R. Babín-Vich[2] and J. M. González-Casado[3]

[1] *ESCET-Área de Geología, Universidad Rey Juan Carlos, C/Tulipán s/n,* 28933 *Móstoles (Madrid), Spain. E-mail: d.gomez@escet.urjc.es*
[2] *Depto. Geodinámica, Universidad Complutense de Madrid, C/Jose Antonio Novais s/n,* 28040 *Madrid, Spain. E-mails: rosatej@geo.ucm.es (RT); jaruiz@geo.ucm.es (JR); rosbabin@geo.ucm.es (RBV)*
[3] *Depto. de Química Agrícola, Geología y Geoquímica, Universidad Autónoma de Madrid, F. de Ciencias, C-VI U. Autónoma de Madrid,* 28049 *Madrid, Spain. E-mail: G.Casado@uam.es*

Accepted 2004 October 11. Received 2004 September 27; in original form 2004 April 2

SUMMARY

Effective elastic thickness of the lithosphere of the Iberian peninsula was estimated from a coherence analysis of topography and gravity spectra, for which a multitaper technique was used. Coherence estimates provide an average T_e value of 17 ± 4 km. To verify the T_e derived from the spectral analysis, we compare it to independent T_e estimates from strength envelopes constructed for some tectonic units located at the interior of the Iberian peninsula. We obtain T_e values ranging from 10 to 25 km. These values are consistent with coherence results. Tectonic evolution of the area involved an Early Mesozoic rifting (Late Permian—Early Cretaceous) and a subsequent period of compression. Present morphotectonic units result from Alpine deformation events (mainly Neogene). No widespread volcanism activity or/and high heat flow values have been reported to have occurred during intraplate domain deformation. The Iberian lithosphere response to loading primarily reflects its pre-existing inherited mechanical structure, which has remained thermally relatively unperturbed.

Key words: continental deformation, crustal structure, Geodynamics, gravity anomalies, rheology.

1 INTRODUCTION

The development of flexural modelling has resulted in several new lines of research designed to explore isostatic compensation mechanisms and the response of lithosphere strength to loading and unloading (e.g. Watts 2001). The isostatic flexural model is one of regional compensation, which assumes that the lithosphere responds to long-term geological loads as an elastic plate that overlies a weak fluid substratum. Loads are partially supported by the strength of the lithosphere, which is characterized by its flexural rigidity or effective elastic thickness (T_e). As Watts (2001) pointed out, the lithosphere acts as a filter that suppresses the large-amplitude, short-wavelength deformation associated with local models of isostasy and allows the passage of the small-amplitude, long-wavelength deformation associated with flexure. Flexure can be inferred from the gravity anomaly that is created by lateral density variations induced by deflection under a load of a density discontinuity, such as the Moho. Applied loads can be external, represented by the topography, or internal, mainly defined as the undulations at a surface compensation, or both (e.g. Forsyth 1985). The gravity anomaly is sensitive to both the load size and the flexural response of the lithosphere. Calculations of T_e in the frequency domain are based on admittance and coherence functions. The admittance function quantifies a linear relationship between gravity and topography, so it can be defined as the linear transfer function that best predicts the Bouguer anomaly in a least-square sense, given the topography (Forsyth 1985). One of the most widely used techniques to calculate in the frequency domain is the coherence method (Forsyth 1985), which evaluates the statistical relationship between the 2-D topography and gravity spectra.

In this study, a multitaper spectral method was used to calculate Bouguer-topography coherence for the Iberian peninsula interior, an intraplate domain deformed in Alpine times.

2 ESTIMATING COHERENCE USING THE MULTITAPER SPECTRAL TECHNIQUE

The admittance $Q(k)$ is computed from the Fourier transforms of topography $H(k)$ and Bouguer anomaly $B(k)$ (Dorman & Lewis (1970), Forsyth 1985):

$$B(k) = Q(k) \cdot H(k), \tag{1}$$

where k is the 2-D wavenumber, defined as $2\pi/\lambda$ in which λ is the wavelength.

In order to minimize the noise, the admittance can be better expressed as (Forsyth 1985)

$$\hat{Q}(k) = \frac{\langle B \cdot H^* \rangle}{\langle H \cdot H^* \rangle}, \quad (2)$$

in which the angle brackets represents averaging over discrete wavenumber bands and the asterisk indicates the complex conjugate.

Forsyth (1985) pointed out the admittance dependence on the loading experienced by the lithosphere and the need to precisely establish the ratio (f) between the applied load at the Moho (internal load) and the applied surface load. To partly avoid errors resulting from an incorrect definition of the f ratio, this author proposed the use of the parameter coherence, whose dependence on the f ratio is much lower.

Coherence is the wavenumber domain analogue of correlation. The squared coherence function $\gamma^2(k)$ between two stochastic processes, in this case the gravity anomaly and topography, is the magnitude squared of the cross-spectral density function of both fields, normalized by the power spectral density functions of the individuals fields E_0 (topography) and E_1 (gravity anomaly; e.g. Forsyth 1985; Simons *et al.* 2000):

$$\gamma^2(k) = \frac{C^2(k)}{E_0(k)E_1(k)}. \quad (3)$$

A typical coherence graph shows a value ranging from 0 at short wavelengths to 1 at long wavelengths. This is because at long wavelengths, topographic loading is fully compensated by Moho deflection, but at short wavelengths, the topography is sustained by the flexural rigidity of the lithosphere with no deflection. The wavelength at which the transition between low and high coherence values occurs is directly related to the T_e of the lithosphere. Thus, the best estimate of T_e for the lithosphere can be made by computing the observed coherence from gravity and topography data sets for a particular area, and comparing it with the predicted coherence for different T_e values.

Here, the multitaper method is used to calculate the power spectral density function (Thomson 1982). A summary of the multitaper method is presented next. A more detailed explanation can be found in Simons *et al.* (2000). This technique provides an optimal spectrum estimate by minimizing spectral leakage while reducing the variance of the estimate by averaging orthogonal eigenspectrum determinations (Lees & Park 1995). In order to do this, ideal data windows need to be obtained, whose spectral responses have the narrowest central lobe and the smallest possible sidelobe level. These ideal data windows are given by prolate spheroidal sequences (Slepian 1978). The width of the central lobe of the spectral responses is a measure of the resolution of the estimates. The half width of the central lobe, W, corresponds to an integer multiple, j, of the fundamental frequency: $W = j/(N \cdot \Delta t)$, N being the total data set length andΔt the sampling interval. Commonly, j is quoted as NW (assuming $\Delta t = 1$) and this parameter usually varies from 2 to 4, determining the resolution of the estimates (Simons *et al.* 2000). Hence, the resolution is defined as $2^*NW/N/\Delta t$. Choosing the appropriate NW value is left to the consideration of the analyst (Simons *et al.* 2000) but a comparison between the results obtained from different NW values is desirable. Progressively higher NW values provide lower resolution, but this also reduces the coherence values both at short and long wavelengths. In addition to this, higher NW values decrease the variance of the resulting estimate, which is really the aim of the multitaper technique. The root square of the variance, the standard deviation, is the value used as the error estimate of the coherence function.

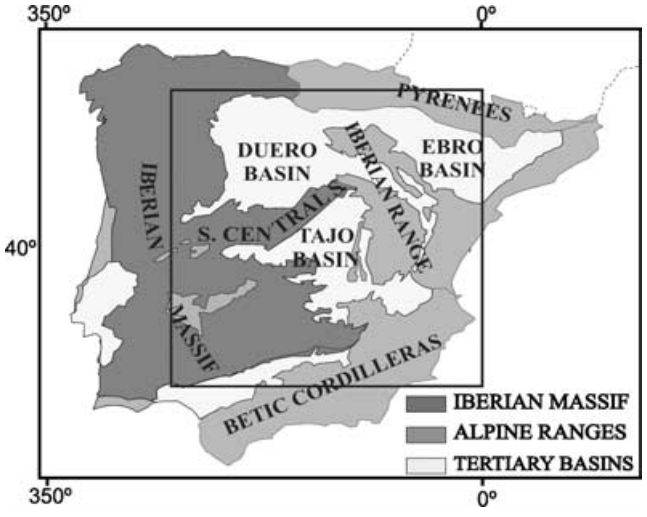

Figure 1. Location map showing the main tectonic units of the Iberian peninsula. Inset shows the study area.

3 GEOLOGICAL SETTING

Today's configuration of the central Iberian peninsula is the result of a series of tectonic events occurring under extensional and compressive regimes. During the Mesozoic, the Variscan crust underwent several extensional episodes that gave rise to a large sedimentary basin, the Iberian basin, in the eastern region of the Iberian peninsula. The convergence of the Eurasian and African plates from the Late Cretaceous onwards led to the formation of two mountain ranges in the active northern and southern borders of the Iberian Plate, and to the Iberian basin inversion. These mountain ranges are the Pyrenees and their extension towards the western Cantabrian range in the north, and the Betic cordilleras in the south (Fig. 1). Foreland basin formation associated with the Pyrenees gave rise on the south side to the Ebro basin and to the Guadalquivir basin in the case of the Betic cordilleras. Within the intraplate domain in the central part of the Iberian peninsula, transmitted compressional stresses gave rise to two mountain ranges: the Spanish Central System trending E-W and NE–SW, and the Iberian range with its NW–SE orientation. The Iberian range developed during the Palaeocene by inversion of the Iberian basin and is characterized by a relatively gentle topography, with mean heights of some 1000 m, above which a few massifs rise to over 2000 m. Towards the west, in a direction transverse to the Iberian range, is the Spanish Central System. This is a crustal block uplifted by two high-angle, reverse faults (e.g. Portero & Aznar 1984; De Vicente *et al.* 1992). Maximum heights are 2600 m, averaging 1150 m. Border reverse faults cause basement rocks to overlie Tertiary sediments that infill the Duero and Tajo basins. In these river basins, continental sediments reach a thickness exceeding 3000 m, their depocentres occupying troughs parallel to the margins of the mountain chains as well as areas nearby (Aeroservice 1964; Querol 1989; Pulgar *et al.* 1995). Towards the east and south of the Duero and Tajo basins is the Iberian massif, an extensive Variscan basement outcrop that forms the western Iberian peninsula.

According to seismic data, crust thickness in the central Iberian peninsula averages some 31 km (ILIHA DSS Group 1993). At the Central System, the crust thickens and the Moho drops to 34 km (Suriñach & Vegas 1988; ILIHA DSS Group 1993). There also appears to be some thickening under the Iberian range (Zeyen & Fernández 1994), for which gravity modelling suggests a crust thickness of 40 km (Salas & Casas 1993).

4 GRAVITY AND TOPOGRAPHY DATA

Two sets of gravity data were used in this study. The first set corresponds to our own data corresponding to 2892 gravity stations covering an area of approximately 23 657 km^2 in central Spain (Gómez-Ortiz *et al.* 2003). All gravity measurements were corrected for routine corrections such as Earth-tide effects, and free-air and Bouger reductions were also applied. In order to obtain complete Bouguer anomaly values, terrain correction up to 166.7 km was also undertaken using a digital elevation model and an algorithm combining the methods described by Kane (1962) and Nagy (1966). All the gravity measurements were made with Lacoste–Romberg (Model G) gravimeters of sensitivity 0.01 mGal. In addition to this, we used data from the Bouguer anomaly map of the Iberian peninsula (Mezcua *et al.* 1996) to extend our study area to a total length of 600 km both in N–S and E–W directions. A comparison of 469 duplicate gravity measurements for the two data sets revealed an rms error of $\pm$ 0.88 mGal, the total range of the Bouguer anomaly map being 210 mGal. This is a very acceptable error for a regional study and indicates that the different data sets can be used together. Gravity data for the small coastal areas at the easternmost points of the study area were taken from Sandwell & Smith (1997). Although these satellite-derived grids do not have a high precision in coastal areas, in this case they cover a small zone within the studied area and we think that they cannot bias the results. The density value used in the Bouguer reduction was 2670 kg m^{-3} (Fig. 2a). The Fig. 2(b) shows the distribution of the terrestrial gravity stations used in this study.

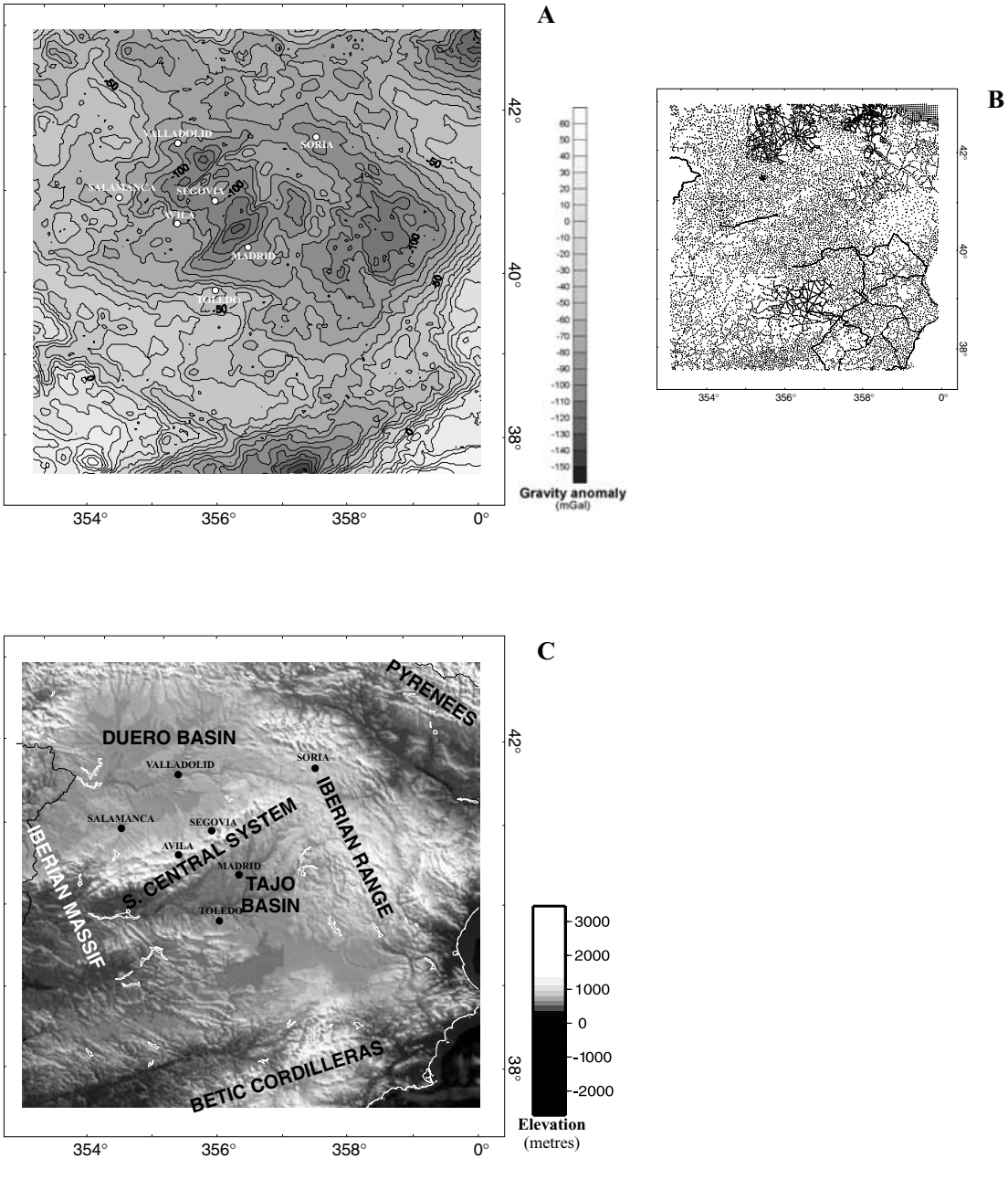

Figure 2. Data set used to calculate the effective elastic thickness: (a) Bouguer anomaly map of the area examined, contour interval 10 mGal; (b) data distribution map with the terrestrial gravity stations used in this study; (c) digital elevation model of the study area derived from topographic data from the GTOPO30.

The topography data (Fig. 2c) were obtained from the GTOPO30 digital elevation model (Gesch *et al.* 1999). Bathymetric data were obtained from the ETOPO5 elevation data set (NOAA 1988). These bathymetric data derived from satellite gravity over the oceans are in part derived by assuming a mechanical model of the oceanic lithosphere but, as only a reduced area of coastal bathymetry is being added to the topography, it is not possible that it invalidates the results. Bouguer gravity and topography data were gridded every 10 km using kriging (Fig. 2), a geostatistical technique that attempts to interpolate data based on their spatial correlation structure (Journel & Huijbregts 1978).

The topography of the Iberian peninsula (Fig. 2c) shows alternating E–W to NE–SW and NW–SE trending mountain chains and river basins. The Bouguer anomaly map identifies a gravity low in the Iberian peninsula interior, in which there is a succession of relative highs and lows trending roughly NE–SW and NW–SE (Fig. 2a). Some spatial relationships can be established from preliminary observation of the gravity and topography maps. Gravity lows correspond, in a broad sense, with the topography highs associated with the Central System and the Iberian range.

5 EFFECTIVE ELASTIC THICKNESS OF THE IBERIAN PENINSULA LITHOSPHERE

Effective elastic thickness of the Iberian peninsula lithosphere was estimated from a coherence analysis of topography and gravity spectra. The gravity response resulting from the combined effects of surface topography and Moho deflection is compared with the observed anomaly. The observed coherence curves are compared with theoretical ones, calculated for different T_e values. The best-fitting model is chosen by error minimization.

Table 1 summarizes the parameters values used in computing the theoretical T_e. Using the *P*-wave velocities described in several reports of refraction seismic of the study area (Banda *et al.* 1981; Suriñach & Vegas 1988; ILIHA DSS Group 1993; Pulgar *et al.* 1995) and converting these to density using the expressions described by Christensen & Mooney (1995), the values obtained for the topographic load density and crust—lithospheric mantle density contrast are 2670 and 440 kg m^{-3}, respectively.

As has been previously described, Forsyth (1985) pointed out that f (top–bottom loading ratio) ranges from 0.1 to 5 but coherence is not very sensitive to these variations. In addition to this, the f parameter has a different value for each wavenumber. Taking this into account, we realize that the assumption of different loading ratios can lead to additional uncertainties in the determined T_e value. In all analyses, the average loading ratio needed to calculate the predicted coherence was held constant at an average value of 1 and all predictions have been made using this constant loading ratio. Coherence was estimated for different *NW* values (2, 3 and 4). As previously mentioned, the resolution of the estimates is defined as $2^*NW/N/\Delta t$, Δt being the sample interval (Simons *et al.* 2000). Thus, in this particular case the resolutions associated to the *NW* values of 2, 3 and 4 are 0.0421, 0.0628 and 0.0836 rad km^{-1}, respectively. Fig. 3 shows

Table 1. Parameters used in the computation of the theoretical coherence.

Parameter	Value
Poisson's ratio, υ	0.25
Young's modulus, E	10^{11} N m^{-2}
Topographic load density	2670 kg m^{-3}
Crust—lithosperic mantle density contrast	440 kg m^{-3}
Mean crustal thickness	31 km

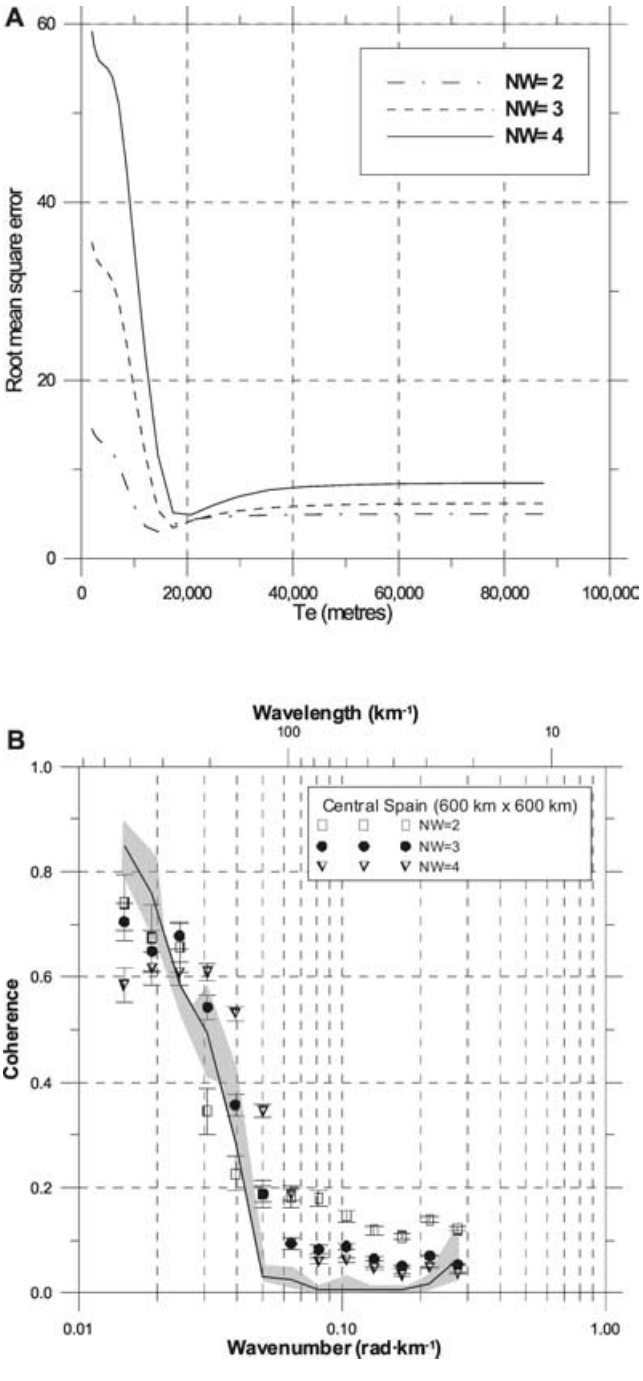

Figure 3. (a) The rms error between the observed and theoretical coherence for three values of *NW*. *NW* is the parameter that determines the resolution of the estimates (see the text for more details). (b) Observed (open squares for $NW = 2$, black circles for $NW = 3$ and open triangles for $NW = 4$) versus theoretical coherence. Theoretical coherences for $T_e = 14$ and 21 km bound the grey area; solid line is the theoretical coherence for $T_e = 17$ km.

coherence graphs and the rms error obtained. As shown in this figure, progressively higher *NW* values provide lower lower coherence values both at short and long wavelengths. The rms error between the observed coherence and the coherence calculated for different *NW* was used to assess reliability of coherence estimate. In addition to this, higher *NW* values decrease the variance of the resulting estimate, which is really the aim of the multitaper method. The rms error value reveals a well-defined minimum at 14 km (Fig. 3a) for

$NW = 2$, 17 km for $NW = 3$ and 21 km for $NW = 4$. From these values, the rms error starts to increase again, becoming stable after T_e values higher than ~ 40 km. Figure 3(b) shows observed versus theoretical coherence for a T_e of 14, 17 and 21 km. As expected from theory, a coherent relationship between topography and Bouguer anomaly does not exist at short wavelengths. The predicted coherence curve corresponding to a $T_e = 17 \pm 4$ km best fits the observed coherence at the transitional wavelength between low and high coherence. The explicit relation between transitional wavelength and loading ratio in function of the T_e has been derived by Simons & van der Hilst (2003). It is important to note that these authors have pointed out that it is not possible to uniquely determine the loading ratio and the T_e based on the coherence alone. Thus, transitional wavelength is an indicator of the characteristic flexural wavelength of the lithosphere elastic plate and a mean T_e of 17 ± 4 km characterizes the Iberian lithosphere. Futhermore, both the lower and the greater T_e estimates are within the error interval for $T_e = 17$ km. In all cases, at long wavelengths the observed coherence is lower than the predicted one. This effect has been previously described (e.g. Simons *et al.* 2000) and can be attributed to several factors, such as the differences between the conditions of the starting crustal model and the real structure, or the difficulty in reducing the indetermination in the relationship between top and bottom loads.

The T_e estimates results show a lower T_e value than expected in a continental intraplate domain. Some authors have suggested that the coherence method using multitaper spectral estimation can yield significant underestimates of the elastic plate thickness (see for example Banks *et al.* 2001; Ojeda & Whitman 2002; Swain & Kirby 2003). Using synthetic data in order to generate grids of topography–gravity sets with predefined T_e values, these authors calculate the observed coherence using different spectral methods (periodogram, multitaper method, maximum entropy method) in order to determine the one that best fits to the theoretical T_e value. Their conclusions are that the multitaper method underestimates the value of T_e more than maximum entropy method when T_e is large, greater than approximately 40 km, because the transition wavelength approaches the window size. Moreover, the difference between the estimated and the true value of T_e increases with T_e. Thus, the T_e value of 17 ± 4 km for the Iberian peninsula interior can be considered as a lower bound. However, the window size used in this study (600×600 km) is small and this implies that using another spectral estimator (for example, maximum entropy method) also would provide a lower bound value. The comparison of this T_e value with other independent estimations, such as rheological profiles, can provide us a clue in order to determine if this value is far from the true one or not.

6 COMPARISON WITH T_e ESTIMATES BASED ON STRENGTH ENVELOPES

To compare our results with independent estimations, we have calculated T_e from strength envelopes constructed by Tejero & Ruiz (2002) for the Duero and Tajo basins, and the Central System (Fig. 4). Under tensional stresses, strength envelopes show two brittle–ductile transitions except for the northern area of the Tajo basin (Fig. 4). The upper one is located within the upper crust at a mean depth of 8 km for wet quartzite and 10 km for dry quartzite. It shallows to 6 km for the wet granite composition of the upper crust of the Spanish Central System. The lower one is located within the middle crust at 16 km depth beneath the basins and at 14 km beneath the mountain range. In compression stress, only a brittle–ductile transition appears and it is restricted to the upper crust. It is shallower beneath the northern area of the Tajo basin, where it is located at 6 km depth for wet quartzite and 8 km for dry quartzite, and deepens to 8 km and 10 km for wet and dry quartzite beneath the Duero basin. All rheological profiles show a ductile lower crust that is always softer than the uppermost mantle.

Following Burov & Diament (1995), the total effective elastic thickness of an unflexed plate constituted by n detached layers is

$$T_e = \left(\sum_{i=1}^{n} h_i^3 \right)^{1/3}, \tag{4}$$

where h_i is the mechanical thickness of the layer i. We take the base of each mechanical (competent) layer as the depth in which the strength goes down to a value of 10 MPa. If strength levels at the base layer are higher than 10 MPa, the layer is considered welded to the layer below. The calculations were performed for both wet and dry rheologies. For the basins, the obtained values are 18–19 km for wet rheologies and 26–27 km for dry rheologies. For the Central System, results are 13 and 22 km for wet and dry rheologies, respectively (Table 2). The lower values for the Central System are greatly the result of the weaker upper mantle, which has a limited contribution to the total strength of the lithosphere.

These values are upper limits to the actual T_e, because plate curvature reduces the effective elastic thickness (Burov & Diament 1995; Watts & Burov 2003). A first-order estimation of this effect in a typical continental crust can be performed from (e.g. Watts & Burov 2003):

$$T_e \approx T_e^* \left\{ 1 - \left[K(1.8 \times 10^5 \,\mathrm{m}^{-1}) \left(1 + 19.5 \,\mathrm{km}/T_e^* \right)^6 \right] \right\}^{0.5 + T_e^*/480 \,\mathrm{km}}, \tag{5}$$

where T_e^* is the effective elastic thickness without flexure (obtained from eq. 4) and K is the curvature of the flexed plate. Using for T_e^* our values obtained with eq. (4) and taking $K = 5 \times 10^{-9}$ m^{-1} (the deflection of the Moho in the central part of the Iberian peninsula; Sánchez-Serrano 2000), we obtain an effective elastic thickness between 14 and 25 km for the basins, and between 10 and 20 km for the Central System (Table 2). These values are consistent with coherence results presented in the previous section.

7 DISCUSSION AND CONCLUSIONS

At the moment, in the study area, previous T_e estimates have been provided by flexural modelling. The proposed T_e values are 10–35 km for the the Ebro basin (Gaspar-Escribano *et al.* 2001), 7 km for the Tajo basin (Van Wees *et al.* 1996), 10 km for the Betic cordilleras (Van der Beek & Cloetingh 1992) and 7–13 km for the Guadalquivir basin (García-Castellanos *et al.* 2002). In general, these T_e estimates are low and consistent with our T_e estimates from coherence analyses that show an average value of 17 ± 4 km for the interior of the Iberian peninsula. Effective elastic thicknesses estimated from strength envelopes are summarized in Table 2. Unflexed lithosphere estimates range from 13 to 27 km and could be considered an upper limit of the flexural rigidity or effective elastic thickness. Topographic load of Central System and thrust loads provoke Iberian lithosphere flexure. Considering a flexed plate by bending, T_e estimates range from 10 to 25 km (Table 2). These values are lower than those calculated for an unflexed plate and can be considered a lower limit of T_e estimates derived from strength envelopes. Coherence results are within these ranges. We conclude that the agreement between the T_e value obtained from multitaper method and the ones derived from independent rheological modelling indicates that the true T_e value must not be very different from our estimate.

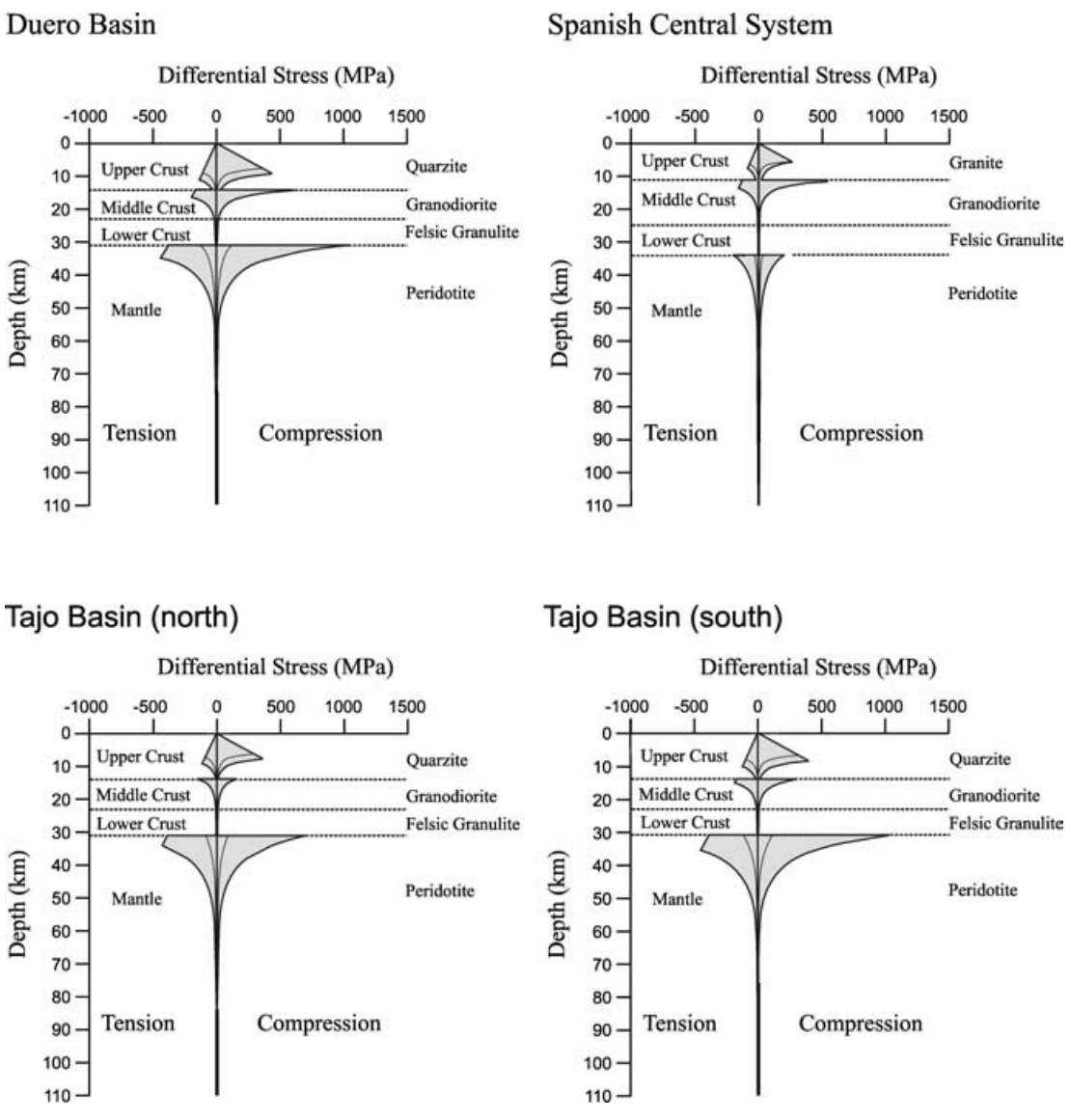

Figure 4. Strength envelopes for the Duero and Tajo basins and Central System. Differential stresses have been calculated in tension and compression at a strain rate of 10^{-15} s^{-1}. Outer black line bounds differential stress estimated for dry rocks composition. Inner black line denotes differential stress for wet rocks composition of the upper crust (quartzite or granite) and lithospheric mantle (peridotite). Heat flow: Duero basin, 60 mW m^{-2}; Central System, 70 mW m^{-2}; Tajo basin, 70 mW m^{-2} (north) and 65 mW m^{-2} (south; see Tejero & Ruiz 2002, for construction details).

Table 2. Summary of T_e values obtained from strength envelopes.

	Unflexed plate T_e (km) wet–dry lithology	Flexed plate T_e (km) wet–dry lithology
Duero basin	18–26	16–24
Central System	13–22	10–20
Tajo basin (north)	16–26	14–24
Tajo basin (south)	18–27	16–25

To a first order, low T_e estimates are related to high heat flow and characterize young thermotectonic provinces (e.g. Watts 2001), although some authors have demonstrated that this is not always true (see for example Simons & van der Hilst 2002). In the study area, present surface heat flow ranges from 50 to 70 mW m^{-2} (Fernández *et al.* 1998). Younger thermal activity corresponds to a hydrothermal cool event that takes place at approximately 20 ± 10 Ma in the eastern part of the Central System (Tornos *et al.* 2000). Only in the south-central part of the studied area a volcanic activity exists. It starts in the Late Miocene and the last volcanic activity takes place at approximately 1.75 Ma (e.g. López-Ruiz *et al.* 2002). Within the Iberian Plate, mountain chains and flanking basins formed in response to collision between the European and African plates. Previously, an Early Alpine rifting took place in the Iberian peninsula (Late Permian—Early Cretaceous). The Iberian Variscan lithosphere underwent extensional deformation and lithospheric thinning. Variscan and Late Variscan structures were reactivated during mesozoic rifting and the lithosphere developed a new mechanical structure. During Alpine compressional episodes, the Iberian lithosphere response to loading must be controlled primarily by its pre-existing inherited mechanical structure, which has remained thermally relatively unperturbed.

Coherence estimates from topography and gravity spectra of the Iberian lithosphere provide T_e values ranging from 14 to 21 km, with an average value of 17 ± 4 km. These values are consistent with T_e

estimates derived from strength envelopes. Low T_e estimates have been attributed to young thermal provinces. In the absence of a young thermal episode, inherited lithosphere structure and tectonic history may play a major role. Future investigations on individual tectonic units may provide a larger data set for the analysis of mechanical properties of the Iberian lithosphere and to constrain T_e estimates.

ACKNOWLEDGMENTS

The authors thank Dr Frederik Simons for providing us with the codes for computing 2-D coherence using the MATLAB program, as well as for his useful comments. We wish to thank two anonymous reviewers and the Editor Dr Yanick Ricard for their constructive comments on the manuscript. We also thank Ana Burton for linguistic assistance. This research was funded by project BTE-2003-03902 (Ministerio de Educación y Ciencia).

REFERENCES

AEROSERVICE, Ltd., 1964. *Aeromagnetic map of Duero Basin,* ITGE, Madrid, Spain.

Banda, E., Suriñach, E., Aparicio, A., Sierra, J. & Ruiz de la Parte, E., 1981. Crust and upper mantle structure of the Central Iberian Meseta (Spain), *Geophys. J. R. astr. Soc.,* **67,** 779–789.

Banks, R.J., Francis S.C. & Hipkin, R.G., 2001. Effects of loads in the upper crust on estimates of the elastic thickness of the lithosphere, *Geophys. J. Int.,* **145,** 291–299.

Burov, E.B. & Diament, M., 1995. The effective elastic thickness (T_e) of continental lithosphere: What does it really mean?, *J. geophys. Res.,* **100,** 3905–3927.

Christensen, N.I. & Mooney, W.D., 1995. Seismic velocity structure and composition of the continental crust: A global view, *J. geophys. Res.,* **100,** 9761–9788.

De Vicente, G. *et al.*, 1992. Alpine structure of the Spanish Central System. In: *III Congreso Geológico de España,* pp. 284–289, SGE-IGME, Salamanca, Spain, .

Dorman, L.M. & Lewis, B.T.R., 1970. Experimental isostasy 1: Theory of determination of the Earth's response to a concentrated load, *J. geophys. Res.,* **75,** 3357–3365.

Fernández, M., Marzán, I., Correia, A. & Ramalho, E., 1998. Heat flow, heat production and lithospheric thermal regime in the Iberian Peninsula, *Tectonophysics,* **219,** 29–53.

Forsyth, D.W., 1985. Subsurface loading and estimates of the flexural rigidity of continental lithosphere, *J. geophys. Res.,* **90,** 12 623–12 632.

García-Castellanos, D., Fernández, M. & Torn´e, M., 2002. Modelling the evolution of the Guadalquivir foreland basin (southern Spain), *Tectonics,* **21**(3), 1–17.

Gaspar-Escribano, J.M. *et al.,* 2001. Three-dimensional flexural modelling of the Ebro Basin (NE Iberia), *Geophys. J. Int.,* **145**(2), 349–368.

Gesch, D., Verdin, K.L. & Greenlee, S. K., 1999. New land surface digital elevation model covers the Earth, *EOS, Trans. Am. geophys. Un.,* **80,** 69–70.

Gómez-Ortiz, D., Tejero, R. & Babín, R., 2003. Estructura de la corteza en el centro peninsular mediante el análisis espectral de datos gravimétricos y modelización en 2 + 1/2D, *Rev. Soc. Geol. de España,* **16**(1–2), 3–17.

ILIHA DSS Group, 1993. A deep seismic sounding investigation of lithospheric heterogeneity and anisotropy beneath the Iberian Peninsula, *Tectonophysics,* **221**(1), 35–51.

Journel, A.G. & Huijbregts, Ch.J., 1978. *Mining Geostatistics,* Acad. Press, New York, p. 600.

Kane, M.F., 1962. A comprehensive system of terrain corrections using a digital computer, *Geophysics,* **27**(4), 455–462.

Lees, J.M. & Park, J., 1995. Multiple-taper spectral analysis: A stand-alone C-subroutine, *Comput. Geosci.,* **21,** 199–236.

López-Ruiz, J., Cebriá, J.M. & Doblas, M., 2002. Cenozoic volcanism I: the Iberian Peninsula, in *The Geology of Spain,* pp. 417–438, eds Gibbons, W. & Moreno, T., Geological Society, London.

Mezcua, J., Gil, A. & Benarroch, R., 1996. *Estudio gravimétrico de la Península Ibérica y Baleares,* Inst. Geográfico Nacional, Madrid, p. 7.

Nagy, D., 1966. The gravitational attraction of a right rectangular prism, *Geophysics,* **31**(2), 362–371.

NOAA, 1988. *Data Announcement 88-MGG-02, Digital relief of the Surface of the Earth,* NOAA, National Geophysical Data Center, Boulder, CO, USA.

Ojeda, G.Y. & Whitman, D., 2002. Effect of windowing on lithosphere elastic thickness estimates obtained via the coherence method: Results from northern South America, *J. geophys. Res.,* **107**(11), 2275, doi:10.1029/2000JB000114.

Portero, J.M. & Aznar, J.M., 1984. Evolución morfotectónica y sedimentación terciarias en el Sistema Central y cuencas limítrofes (Duero y Tajo). In: *I Congreso Español de Geología,* pp. 253–263, SEG-IGME, Madrid, Spain.

Pulgar, J., Perez-Estaun, A., Gallart, J., Alvarez-Marron, J., Gallastegui, J., Alonso, J.L. & ESCIN group, 1995. The ESCI-N2 deep seismic reflection profile: a traverse across the Cantabrian Mountains and adjacent Duero basin, *Rev. Soc. Geol. España,* **8**(4), 383–394.

Querol, R., 1989. *Geología del subsuelo de la Cuenca del Tajo,* E.T.S.I. Minas de Madrid (Dpto. de Ingeniería Geológica), Madrid, Spain, p. 48.

Salas, R. & Casas, A., 1993. Mesozoic extensional tectonics, stratigraphy and crustal evolution during the Alpine cycle of the eastern Iberian basin, *Tectonophysics,* **228,** 33–55.

Sandwell, D.T. & Smith, W.H.F., 1997. Marine gravity anomaly from Geosat and ERS 1 satellite altimetry, *J. geophys. Res.,* **102,** 10 039–10 054.

Sánchez-Serrano, F., 2000. Análisis de la Topografía y Deformaciones Recientes en el Centro de la Península Ibérica, *PhD thesis,* University Complutense de Madrid, Madrid, Spain.

Simons, F.J. & van der Hilst, R.D., 2002. Age-dependent seismic thickness and mechanical strength of the Australian lithosphere, *Geophys. Res. Lett.,* **29**(11), doi:10.1029/2002GL014962.

Simons, F.J. & van der Hilst, R.D., 2003. Seismic and mechanical anisotropy and the past and present deformation of the Australian lithosphere, *Earth planet. Sci. Lett.,* **211,** 271–286.

Simons, F.J., Zuber, M.T. & Korenaga, J., 2000. Isostatic response of the Australian lithosphere: Estimation of effective elastic thickness and anisotropy using multitaper spectral analysis, *J. geophys. Res.,* **105,** 19 163–19 184.

Slepian, D., 1978. Prolate spheroidal wave functions, Fourier analysis and uncertainty, V, The discrete case, *Bell. Syst. Tech. J.,* **57,** 1371–1429.

Suriñach, E. & Vegas, R., 1988. Lateral inhomogeneities of the Hercynian crust in central Spain, *Phys. Earth planet. Int.,* **51,** 226–234.

Swain, C.J. & Kirby, J.F., 2003. The effect of 'noise' on estimates of the elastic thickness of the continental lithosphere by the coherence method, *Geophys. Res. Lett.,* **30**(11), 1574, doi:10.1029/2003GL017070.

Tejero, R.M. & Ruiz, J., 2002. Thermal and mechanical structure of the central Iberian Peninsula lithosphere, *Tectonophysics,* **350,** 49–62.

Thomson, D.J., 1982. Spectrum estimation and harmonic analysis, *Proc. IEEE,* **70,** 1055–1096.

Tornos, F., Delgado, A., Casquet, C. & Galindo, C., 2000. 300 Million years of episodic hydrothermal activity: stable isotope evidence from hydrothermal rocks of the Eastern Iberian Central System, *Mineral. Deposita,,* **35**(6), 551–569.

Van der Beek, P.A. & Cloetingh, S., 1992. Lithospheric flexure and the tectonic evolution of the Betic Cordilleras (SE Spain), *Tectonophysics,* **203,** 325–344.

Van Wees, J.D., Cloetingh, S. & De Vicente, G., 1996. The role of pre-existing faults in basin evolution: constraints from 2D finite element and 3D flexure models, in *Modern developments in Structural interpretation, Validation and Modelling,*Vol. **99,** pp. 297–320, eds Buchanan, P.G. & Nieuwland, D.A., Geol. Soc., London.

Watts, A.B., 2001. *Isostasy and flexure of the lithosphere,* Cambridge Unversity Press, London, p. 458.

Watts, A.B. & Burov, E.B., 2003. Lithospheric strength and its relation to the elastic and seismogenetic layer thickness, *Earth planet. Sci. Lett.,* **213,** 113–131.

Zeyen, H. & Fernández, M., 1994. Integrated lithospheric modelling combining thermal, gravity, and local isostasy analysis: Application to the NE Spanish Geotransect, *J. geophys. Res.,* **99,** 18 089–18 102.